Macromolecules

ARTICLE

pubs.acs.org/Macromolecules

Architectural Dispersity in Model Branched Polymers: Analysis and Rheological Consequences

Frank Snijkers,[†] Evelyne van Ruymbeke,[†,‡] Paul Kim,[§] Hyojoon Lee,[§] Anastasia Nikopoulou,[⊥] Taihyun Chang,[§] Nikos Hadjichristidis,[⊥] Jai Pathak,[†,○] and Dimitris Vlassopoulos*[,†,∥]

[†]FORTH, Institute of Electronic Structure & Laser, Heraklion, Crete, Greece

[‡]Bio and Soft Matter, Institute on Condensed Matter and Nano-science, Université catholique de Louvain, Louvain-la-Neuve, Belgium

[§]Department of Chemistry and Division of Advanced Materials Science, Pohang University of Science and Technology, Pohang, 790-784, Korea

[⊥]Department of Chemistry, University of Athens, Athens, Greece

[∥]Department of Materials Science & Technology, University of Crete, Heraklion, Crete, Greece

ABSTRACT:

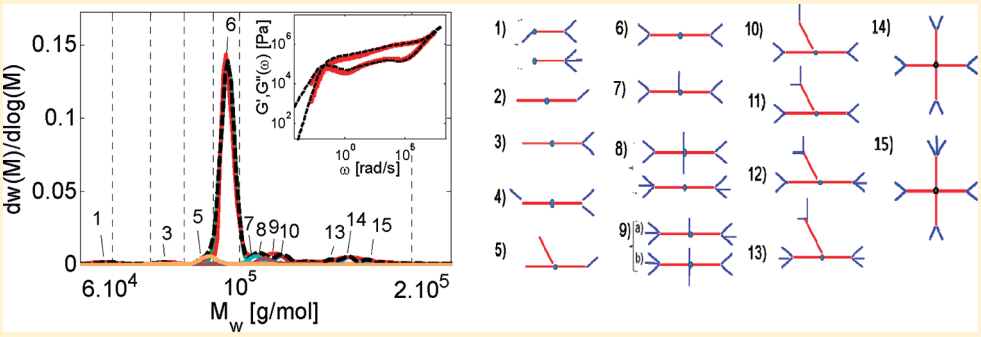

We combine state-of-the-art synthetic, chromatographic, rheological, and modeling techniques in order to address the role of architectural polydispersity in the rheology of model branched polymers. This synergy is shown to be imperative in the field and leads to several important results. Even the best available synthesis is prone to "contamination" by side-products. The exact targeted macromolecular structure can be analyzed experimentally and statistically and eventually fractionated. Temperature-gradient interaction chromatography proves to be an indispensible tool in this process. All techniques are sensitive to the various macromolecular structures, but in different ways. In particular, the presence of side-products may or may not influence the linear rheology, due to competing contributions of the different relaxation processes involved, reflecting different structures at different fractions. Hence, combination of all these techniques is the key for fully decoding the architectural composition of branched polymers and its influence on rheology.

I. INTRODUCTION

In the last 2 decades, we have witnessed a remarkable progress in the understanding of the rheology of branched polymers.[1−13] The key ingredient that catalyzed the developments in this field is the wise synergy of state-of-the-art chemistry (high-vacuum anionic synthesis), physical experiment (rheology) and modeling (tube-based). Here we focus on linear viscoelasticity. With the help of well-defined and masterfully produced model branched polymers (such as H, combs, dendritically branched Cayley trees, pom-poms) their viscoelastic relaxation mechanisms have been established: these complex macromolecules relax their stress hierarchically, from the outer to the inner parts.[2,5,13] Once an outer part (layer) with free dangling ends is relaxed, it acts as effective solvent for the yet-unrelaxed, stress-carrying inner parts. The latter are diluted, leading to a reduced number of entanglements, and hence relax faster. After relaxation of an outer layer and before the next layer responds, the branch points move within the diluted tube via a hopping mechanism. All these aspects are accounted for in tube-model theories[7,12,14] and, despite debatable issues dealing primarily with the dilution exponent and the extend of branch point hopping, the predictions are on the overall in excellent quantitative agreement with the experimental data. Note that once the latter two issues are accounted for (by choosing fixed values for the so-called dilution exponent α, and p^2 parameter), the models are parameter-free as the additional input parameters (plateau modulus, molar mass between entanglements and Rouse time of entanglement segment) can be obtained from the rheological data of the test

Received: June 21, 2011
Revised: August 31, 2011
Published: October 05, 2011

samples. This gives confidence for the above approach and in addition points to the importance of the uniquely obtained model macromolecular architectures in understanding the physics of branched polymers. Consequently, it is possible to understand complex flows of complex polymers[15,16] and eventually optimize industrial processes.

Despite the above advances, one often experiences situations where for the same series of model homopolymer samples the comparison between model predictions with fixed input parameters may vary from excellent to poor. Examples from our own work have been discussed in the literature in the context of comb[13,17] and Cayley-tree polymers.[6] There, it was suggested that in addition to the very small size polydispersity, which can be accounted for, some structural polydispersity is possible, in fact expected for these architecturally complex macromolecules, even when the best possible synthetic approach has been used. It was even shown that by considering plausible architectural side-products in small fractions (empirically) improved predictions could be obtained.

In addition, tube-based models proved themselves to be sufficiently accurate in order to be used as complementary tools for the so-called inverse problem, i.e., characterizing a complex polymer. For example, it has been shown that combining these models with viscoelastic data and size-exclusion chromatography (SEC), it is possible to detect the presence of long chain branching.[18−21] Because of its high sensitivity to tiny amounts of high-molecular weight chains, often rheology is shown to be more accurate than SEC techniques, the results of which are known to vary within a factor around 10%. Hence, while tube-models have been developed based on the assumption that model samples were architecturally monodisperse, they can now help to better understand the real composition of these model samples and to validate their experimental polydispersities. To determine the latter, additional sensitive characterization techniques are necessary. It turns out SEC is not an adequate characterization technique for, e.g., comb polymers. The reason is that combs with different numbers of arms could have similar hydrodynamic radii, and hence cannot be separated with the low resolution technique due to the large band broadening.[22]

The breakthrough in this direction came with the development of the temperature gradient interaction chromatography (TGIC).[23,24] This technique can separate such polymers because it is sensitive to total molecular weight and has a much higher resolution compared to SEC.[22] Recently, it was demonstrated that combination of TGIC, rheology and modeling allows obtaining the distribution of the number of arms in comb polystyrenes.[25] It turns out that architectural dispersity has a great influence on the rheology. Perhaps the strongest evidence is the extreme case of ring polymers, where the presence of linear uncoupled chains in fraction below 0.1% can alter their response dramatically.[26] On the basis of these advances, very recent work on H-polybutadienes demonstrated the power of TGIC and allowed properly analyzing the model samples with structural dispersity.[27]

The above examples suggest that the synergy of synthesis, rheology and modeling should be complemented with advanced characterization techniques such as TGIC for a complete understanding of branched polymer rheology.

The objective of the present work is to combine all tools available, experimental and theoretical alike, in order to determine the real composition of model branched polymers and its consequences on the rheology. To this end, we use recently synthesized model exact comb polymers,[28] where the position of a branched point is well-defined. Created from the association of several parent linear chains, these molecules, which contain two or three branches at specific positions along a well-defined backbone, represent a real challenge in synthesis, and side-products cannot be avoided. We determine these side-products and their fractions, and discuss their importance on the viscoelastic properties of the samples. We employ SEC and TGIC. By combining with rheology and modeling, and comparing the unfractionated and fractionated exact-comb polybutadienes, we also address the validity limit of the different techniques (synthesis, SEC, TGIC, tube-based model). The modeling approach we use in this work is largely based on analysis of the rheology of pure components (fractions) of the mixture (comb polymer) analyzed by TGIC. This captures the experimental rheology very well.

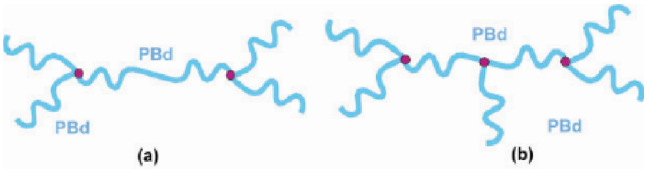

Figure 1. Illustration of exact comb PBds with (a) two identical branches (C-2 or H-type PBd, α-comb) and (b) three identical branches, H-type, with an extra identical branch at the middle of the connector (sC-3 PBd, β-comb).

The manuscript is organized as follows: in section II, the synthesis is reviewed and the fractionation of the exact combs as well as their main molecular characteristics are presented. The different experimental techniques used in this work are also briefly described. Section III presents the statistical approach that we developed for determining the composition of the samples from their experimental molecular weight distribution, as well as an overview of the tube model used for predicting their linear rheology. The results are presented and discussed in section IV, and conclusions are presented in section V.

II. EXPERIMENTAL SECTION

II.1. Synthesis and Characterization. The synthesis of the exact combs with two or three identical branches (Figure 1) is given in detail in a previous publication.[28]

Briefly, the synthetic methodology involves (i) the replacement of the two chlorines of 4-(dichloromethylsilyl) diphenylethylene (DCMSDPE) with 3-arm star PBd (C-2 or H-type PBd, thereafter coded as α-comb, Scheme 1) and (ii) the addition of *s*-BuLi to the double bond of DPE followed by polymerization of butadiene from the newly created anionic site (sC-3 or grafted-H, thereafter coded as β-comb, Scheme 1). Intermediate and final products were characterized via SEC, low angle laser light scattering (LALLS) and ^{1}H NMR spectroscopy.[28] The main molecular characteristics are given in Table 1.

The microstructure of the final products, determined by ^{1}H NMR ($CDCl_3$ at 25 °C) was 87−90% 1,4 and 13−10% 1,2.

II.2. Molecular Weight and Architectural Distribution. As mentioned in the Introduction, even the state-of-the-art synthesis of complex macromolecules, such as in the present work, cannot avoid the formation of side-products in the form of different architectures. This is mainly due to the difficulty in controlling the precise stoichiometry between the carbanions and functional groups in DCMSDPE, and the not-high-enough contrast in the reactivities of two chlorosilyl groups and a vinyl

Scheme 1. General Reactions, According to the Methodology Discussed in the Text, for the Synthesis of C-2 or H-type (α-comb) and sC-3 or Grafted-H (β-comb) PBds

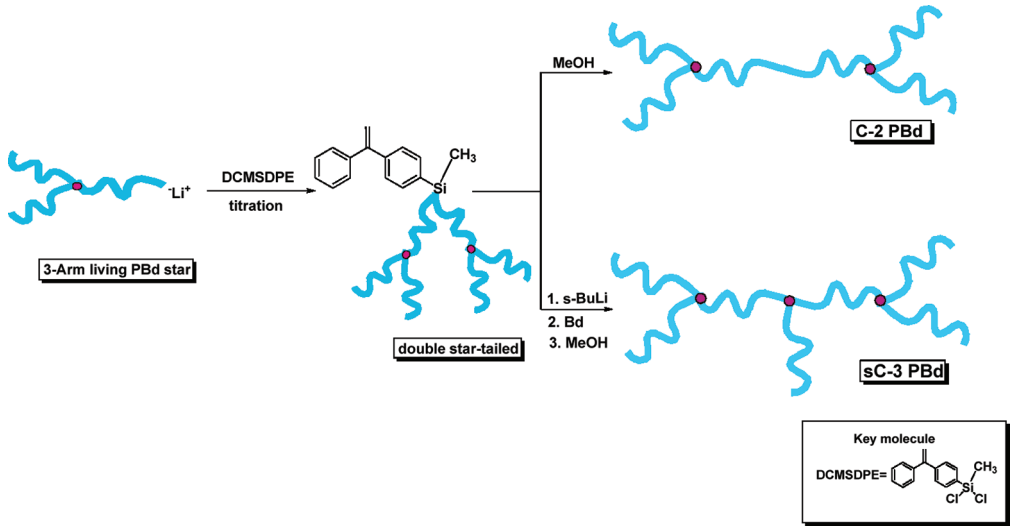

Table 1. Main Molecular Characteristics of Exact Comb PBd Samples Used, from Reference 28 (before Interaction Chromatography Analysis)

	PBd branch			exact comb PBd	
sample	M_w,[a] g/mol	M_w,[b] g/mol	M_w/M_n[a]	M_w,[b] g/mol	M_w/M_n[a]
α-comb	11 400	11 000	1.02	94 400	1.04
β-comb	11 400	11 000	1.02	104 400	1.09

[a] Size exclusion chromatography (SEC) in $CHCl_3$ at 25 °C, using PS standards and corrected for PBd. [b] LALLS in cyclohexane.

group in DCMSDPE. TGIC is sensitive to these side-products but the challenge is to assign the correct structure and to fractionate pure branched polymer species.

SEC Analysis. Two mixed bed columns (Polymer Lab. PL gel mixed C, 300 × 7.5 mm i.d.) were used at a column temperature of 40 °C. SEC chromatograms were recorded with three detectors: light scattering (Wyatt, TREOS), refractive index (Shodex, RI-71), and UV absorption (Thermoscientific, Spectrasystem UV2000) detectors. The solvent was THF (Samchun, HPLC grade) at a flow rate of 0.8 mL/min. Polymer samples for the SEC analysis were dissolved in THF at a concentration of ~1 mg/mL, and the injection volume was 100 μL.

TGIC Analysis. For the reversed phase (RP) TGIC analysis, a C18 bonded silica column (Kromasil C18, 5 μm, 300 Å pore, 150 × 4.6 mm i.d.) was used. The mobile phase was 1,4-dioxane (Samchun, HPLC grade) at a flow rate of 0.5 mL/min. The temperature of the column was controlled by circulating fluid from a programmable bath/circulator (ThermoHaake, C25P) through a homemade column jacket. The sample solutions (~5 mg/mL) were prepared by dissolving the polymers in a small volume of eluent and the injection volume was 100 μL. The chromatograms were recorded with a LS detector (Wyatt, Tristar) and a RI detector (Shodex, RI-101) for online determination of absolute molecular weight of polymers.

IC Fractionation. The polymers were fractionated with the same column and the same solvent at the same flow rate as in the TGIC analysis. Waters 515 HPLC pump was used for solvent delivery and the chromatogram was monitored by a UV absorption detector (KNAUER, K-2051) operated at 230 nm. The injection sample concentration was 10 mg/mL.

Instead of temperature gradient elution, isothermal elution at 22 °C was used to reduce the time required to cool the column back to the initial temperature for repeating fractionations. At the column temperature, the target fraction (the major peak) was well resolved. In the isothermal elution, however, the high MW species eluted very slowly and 1 mL of THF was injected right after the collection of the target fraction. The small amount of THF could flush out the high MW residue effectively from the column so that the next fractionation cycle could be followed quickly.

The fractionation process was repeated automatically by a homemade software based on LabVIEW^{TM} 2009 which controls a sample injector (electronically controlled 2-position, 10-port switching valve, Alltech, SelectPro) connected to a 100 μL loop and a syringe Pump (New Era Pump Systems, NE-1000), a THF injector (Alltech, SelectPro) connected to a 1 mL loop and a syringe Pump (New Era Pump Systems, NE-1000) and collection of the fractionated effluent as well as data acquisition (National Instrument, PCI-2660). A small amount of antioxidant (BASF, Irganox 1010) was added into the collection bottle to protect polymers from oxidation. The collected fractions were concentrated by evaporating the solvent and precipitated in chilled methanol. The final products were dried in a vacuum oven at room temperature.

II.3. Rheology. The linear viscoelastic response was probed with small-strain-amplitude oscillatory shear measurements, which were performed on an ARES-2KFRTN1 strain-controlled rheometer equipped with a force rebalance transducer (from TA, formerly Rheometric Scientific, USA). Invar (a copper/nickel alloy with small thermal expansion coefficient) parallel plates of diameter 8 mm were used. Temperature control was achieved with an accuracy of ±0.1 °C by use of an air/nitrogen convection oven. A liquid nitrogen Dewar was used for measurements at temperatures below ambient. For the higher temperatures, nitrogen gas was fed into the oven to reduce the risk of degradation.

dx.doi.org/10.1021/ma2013805 |*Macromolecules* 2011, 44, 8631–8643

The samples were simply positioned on the bottom plate and then compressed with the rheometer at temperatures around 50 °C. After a stabilization time, the samples were trimmed with a spatula and slightly further compressed. The final height was always between 0.8 and 1.3 mm. Dynamic rheological measurements were carried out in the temperature range −80 to +130 °C, first at temperatures below 50 °C and then at the higher temperatures. The thermal expansion of the plates was always taken into account when changing temperature by making the appropriate changes in gap spacing. The measurements at high temperatures were performed as fast as possible and sample stability was always checked by testing the reproducibility of the measurements at 50 °C. At each temperature, dynamic time sweep and strain sweep experiments were conducted to ensure thermal equilibrium of the sample and to determine the linear viscoelastic region. The time−temperature superposition principle was used in order to combine frequency sweep experiments at different temperatures and to create the master curve. All data presented here are shifted toward a reference temperature T_{REF} of 20 °C. The vertical shift factors are determined from the change of density with temperature:[29] $b_T = (\rho(T_{REF})T_{REF})/(\rho(T)T)$, with T the temperature in K and with the temperature dependence of the density (ρ in g/cm^3) taken from Zoller and Walsh:[30] $\rho(T) = 1.055 - 5.6 \times 10^{-4}T + 5.33 \times 10^{-21}T^2$. The horizontal shift factors result from the least-squares fit as done by the Orchestrator software. The horizontal shift factors can be fitted with the WLF equation[29] $\log(a_T) = (-C_1(T - T_{REF}))/(C_2 + T - T_{REF})$, and with T_{REF} = 20 °C the following parameters result: C_1 = 4.8 and C_2 = 180 °C. When compared at the same reference temperature, these values are in line with literature values for polybutadiene (e.g., ref 13). The glass transition temperatures T_g were measured for both samples with differential scanning calorimetry (PL-DSC, from TA, USA) and they were found to be −91 ± 1 °C for both samples (heating/cooling rate was 5 °C/min). When shifted to T_g, the parameters of the WLF equation become[29] $C_{1,g}$ = 12.5 and $C_{2,g}$ = 69 °C, which are consistent with reported literature values[13] (see also discussion in section IV.2 below).

III. THEORETICAL ANALYSIS

The tube-based model developed by van Ruymbeke et al.[6,7,31] has been used in order to predict the linear viscoelastic properties of the fractionated and unfractionated exact comb polymers. To predict the properties of the freshly synthesized combs, the model, which is briefly described in section III.2, requires prior knowledge of the statistical composition of the sample. To determine the latter, we developed a statistical approach, which is inspired by earlier work[21] and presented in section III.1. below.

III.1. Analysis of Molecular Weight Distribution (MWD). Simply put, inspired by the synthetic route, we can consider that the necessary building blocks for creating the exact combs are branches and/or half-backbones. This is schematically illustrated in Figure 2, where different colors are meant to distinguish branches from backbones (all being polybutadienes here). Note that this does not represent a synthetic methodology (as shown in Scheme 1), but rather the ingredients of the combs, which affect the rheology, as discussed below. Hence, one might expect that all different side-products can be decomposed into branches and half-backbones (or combinations thereof). This strongly reduces the possibilities for describing their corresponding MWD.

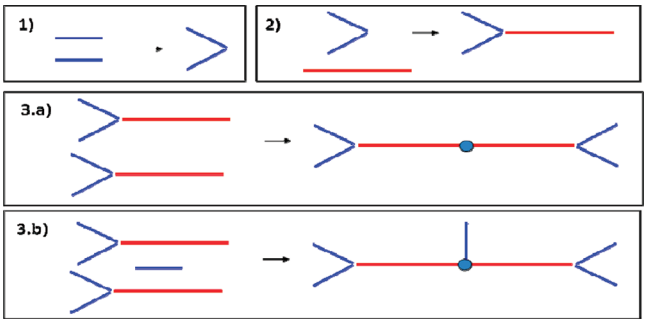

Figure 2. Illustrative construction of the exact combs α (3.a) and β (3.b) from their building blocks, i.e., the branches and the half-backbones (2). This is not a synthetic methodology (as depicted in Scheme 1).

Indeed, starting from the MWD of the branches and of the half-backbones, the MWD of any side-product can be statistically determined. This, in turn, requires determining the MWD of a side-product k obtained by combining two kinds of molecules, i and j, for which we know the MWD (experimentally or statistically). For example, if chains i and j represent two different branches, the chain k will correspond to the pair of two branches (Figure 2, part 1). Further, if chains i and j represent the pair of two branches (whose MWD was just determined statistically) and a half-backbone respectively, chain k will be the half of the exact comb polymer α (Figure 2, part 2). Following this path, the MWD of all possible side-products can be built, step by step, starting from the simplest ones (e.g., the combination of one branch/half- backbone with another branch/half-backbone) to "supra-molecules" based on the association of many branches and half-backbones.

In order to build the MWD of the species k from the MWD of the species i and j, the latter are first decomposed into 20 different fractions with an average molecular weight (in weight) M_i (or M_j) and a weight fraction w_i (or w_j). Then, all possible combinations between chains i and j are taken into account. In order to determine the probability of a specific combination between a chain i of mass M_i and a chain j of mass M_j, its number probability, $p_{\#}(M_i,M_j)$, is calculated from the number probability, $p_{\#,i}$, of each species:

$$p_{\#,i} = \frac{\dfrac{(w_i/\sum_k w_k)}{M_i}}{\sum_k \left(\dfrac{w_k/\sum_n w_n}{M_k} \right)} \quad (1)$$

$$p_{\#}(M_i,M_j) = p_{\#,i} \times p_{\#,j} \quad (2)$$

Probabilities in number are considered since the probability of a chain i or a chain j to become part of a chain k only depends on their living chain ends and not on their length. Their corresponding weight probability, $p_w(M_i,M_j)$ is determined from $p_{\#}(M_i,M_j)$ as follows:

$$p_w(M_i,M_j) = \frac{p_{\#}(M_i,M_j)(M_i + M_j)}{\sum_{l,m} p_{\#}(M_l,M_m)(M_l + M_m)} \quad (3)$$

From eq 3, the weight fraction w_k associated with the chain k with a molecular weight of M_k is easily determined by summing up all the

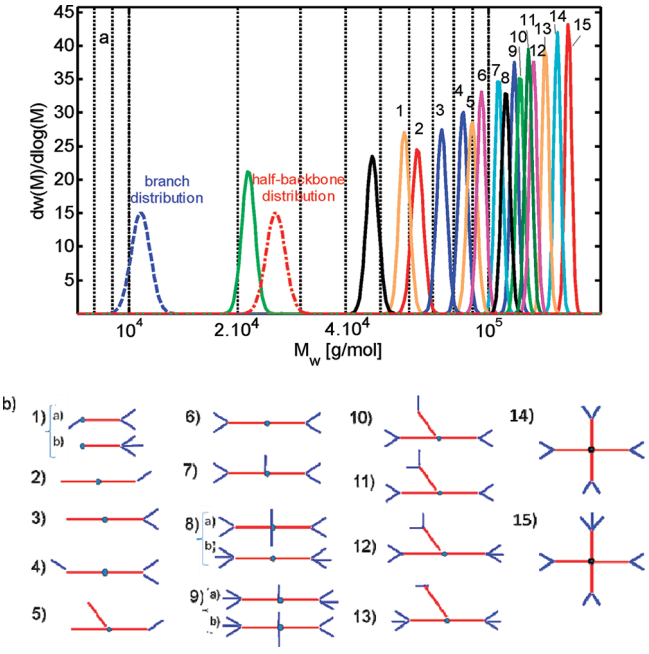

Figure 3. MWD (a) of different possible side-products, identified in (b) and determined from the statistical approach described in eqs 1−3, and considering log-normal distributions with M_w = 10.8 kg/mol and 25.6 kg/mol for describing the distribution of the branches and half-backbones, respectively. Note that all structures are feasible from the synthetic procedure, however the probability for some of them is extremely low (see also text).

probabilities $p_w(M_i,M_j)$ for which $M_i + M_j = M_k$ (note that in eq 4, both $p_{\omega w}(a,b)$ and $p_w(b,a)$ must be considered).

On the basis of this algorithm, which has been validated in ref 21, the MWDs of all possible side-products are determined from the MWDs of the branches and the half-backbones, without any additional degree of freedom. A representative example is shown in Figure 3a, where the MWD of different species have been determined, based on the MWD of the branches and half-backbones and by considering their distribution as a log-normal distribution with M_w = 10.8 kg/mol and 25.6 kg/mol, respectively, and a polydispersity of 1.004 (obtained by fitting the experimental data, see section IV.1 below). These values are consistent with those in Table 1. In Figure 3a, the MWD of each species has been normalized such as:

$$\int_{-\infty}^{+\infty} \frac{\mathrm{d}w\ (\log(M))}{\mathrm{d}[\log(M)]}\,\mathrm{d}[\log(M)] = 1 \qquad (4)$$

The various architectures (combinations of i and j into k) corresponding to these different peaks are illustrated in Figure 3b.

In Figure 3a, we can observe that the polydispersity of the side-products is decreasing with increasing total molecular weight (peaks become narrower, although one has to check both the log-M_w and linear-M_w representations and compare against analysis, as discussed below). This effect, which comes from an averaging effect of the shorter chains with the longer chains (exhibiting a Poisson distribution), has already been observed previously in experimental data.[25,27,32] Since the polydispersity of the parent branches and half-backbones is fixed to 1.004 in order to fit the experimental TGIC curves (see section IV.1), the polydispersity of side-products with a high molecular weight is so small that it should be below the limit of the TGIC technique, and certainly of the SEC. This will be further discussed in section IV.1.

We have validated the above approach by changing the number of slides in the initial parents, or by building the molecules in different ways. For example, we considered two ways of building the β-comb molecule: (i) β-comb=α-comb + one branch, and (ii) β-comb = structure 4 (Figure 3b) + two branches. The final results were always the same. The current approach is thus robust and unambiguous. It is also appropriate for the present description of MWD (discrete points) and for modest computational power.

On the basis of this statistical approach, it is possible to determine the proportions of each possible species in the freshly synthesized mother samples, by fixing them in order to minimize the difference between the experimental MWD of a given sample and the MWD obtained by summing up the MWDs of the various species taken in the proposed proportions. In such a way, the composition of the overall sample is estimated and can be used in order to model its linear viscoelastic properties (LVE). Note, however, that this approach does not allow distinguishing between two different architectures with the same total molecular weight.

III.2. Tube-Based Modeling. The approach used here to predict the linear rheology of the exact comb molecules has been described in detail in the literature.[6,7,31] The main idea is to use an algorithm that defines, for each time step, the survival probability of each initial tube segment along the chain in order to determine the evolution of the total unrelaxed fraction of the polymer melt through time. Each molecular segment can relax by three different mechanisms: reptation, which includes additional friction coming from the branches of the exact comb molecule, contour length fluctuations (CLF), and constraint release (CR). CLF are treated in such a way as to ensure the continuity from the branches of the polymer to the inner part of the backbone. In fact, we use a particular coordinate system for localizing a molecular segment of the backbone, moving from the end of a branch (corresponding to $x = 0$) to the middle of the molecule where $x = 1$.[6,7,31] While the CLF of the inner part of the backbone are slowed down by the extra friction coming from the branches fixed at the extremities of the inner backbone, the middle branch of the exact comb β will speed up this CLF process, since it only brings a larger dilution effect without affecting the fluctuations of the inner backbone. On the other hand, the CR mechanism is considered as a global effect, which increases the molecular weight of the segment between two effective entanglements, $M_e(t)$, yielding a modified "equilibrium state" of the polymer (defined by M_e, the tube diameter a, and the equilibrium length of the molecule L_{eq}). As a consequence, reptation, which is proportional to L_{eq}^2, and CLF, which depends on M_e, are accelerated, due to the dynamic tube dilution (DTD); note here that the full DTD picture is invoked and the p^2 parameter is fixed to 1. We used a dilution exponent α of 1, consistent with earlier works.[5,6,13,33−35]

In what follows, the modeling concerns mainly the analysis of the rheology of the pure fractions (see Figure 3) of the comb samples analyzed by TGIC. This describes the experimental rheology of the exact combs accurately. Some selected examples of modeling mixtures of the main fractions will be presented in section IV.2.2.1 as well.

IV. RESULTS AND DISCUSSION

In order to determine the composition of the two model exact combs α and β, two approaches are tested and confronted, in reference to both the mother and the purified samples. The first is

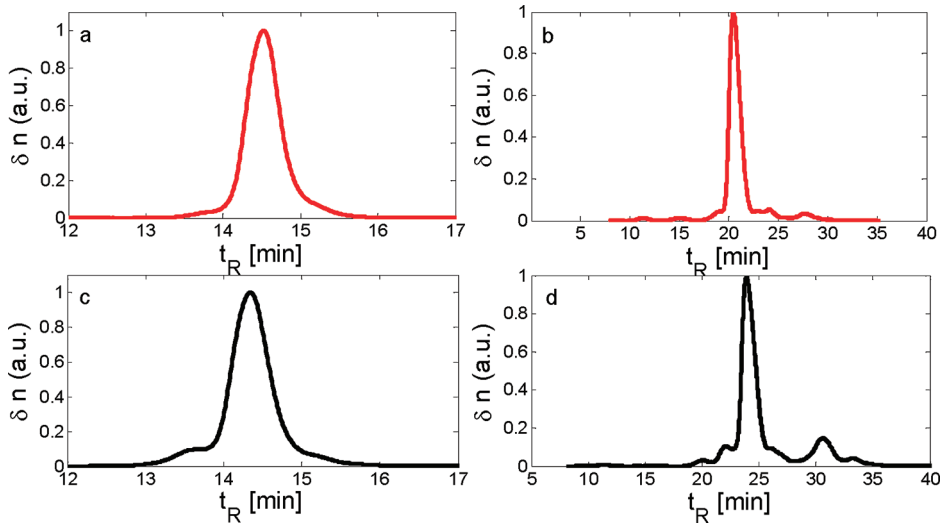

Figure 4. Distribution of the exact comb polymer α determined by SEC (a) and TGIC (b) as a function of elution time. Distribution of sample β determined by SEC (c) and TGIC (d) as a function of elution time. Note that in TGIC the high elution times correspond to high molecular weights, as opposed to SEC.

based on the analysis of their MWDs with the help of the statistical approach described in section III.1, whereas the second is based on the analysis of their linear viscoelastic curves, with the help of the tube-based model described in section III.2.

IV.1. Molecular Weight Distribution. *IV.1.1. Experimental MWD of the Mother Samples and Calibration Curves.* Figure 4 depicts the molecular weight distributions of the mother exact comb polymers α and β, as experimentally determined by SEC (a, c) and TGIC (b, d).

As shown in Figure 4, parts a and c, the SEC data reveals the presence of side products in the unpurified samples. Note that, by "unpurified" we mean samples properly characterized by standard means (as discussed in section II.1) but not fractionated by IC. In particular, a large shoulder appears at low elution times in sample β, which roughly corresponds to species with a molecular weight two times larger than expected. Comb α also shows a small fronting indicating the presence of high molecular weight side products, but this has been often disregarded in the SEC analysis. Extra tailing is also observed at high elution times for both combs, which corresponds to low molecular weight side products including half-molecules. The TGIC data clearly indicate the presence of several synthetic side-products, in addition to those with half or double molecular weight of the target macromolecular structures. Although not in disagreement with the SEC data, the results obtained by TGIC provide a more accurate description of the sample composition. In particular, they reveal that the main peak corresponding to samples α and β (target structures) represent about 85% and 60% of the whole mother samples, respectively. In addition, they allow a more detailed comparison between the compositions of the combs α and β. Therefore, the TGIC data will be used in order to statistically interpret the different components in the samples and their corresponding proportions.

In order to compare theoretical and experimental distributions, the latter must be converted into functions of molecular weights rather than retention times. This is done by calibration. It should be noted that, the TGIC retention varies with experimental conditions, in particular with the temperature program,[24] and the calibration curve, MW vs retention time, needs to be determined for individual separation condition (see Figure 5). Figure 5 depicts the calibration curves of the two exact combs. The calibration curves were obtained by fitting the retention times of identifiable peaks and their corresponding molecular weight with a fifth order polynomial. It can be observed that the molecular weights of the exact combs side-products can vary significantly and as a result a polynomical fitting appears better than a simple linear relationship between retention time and the logarithm of their mass, contrarily to what was proposed recently.[27]

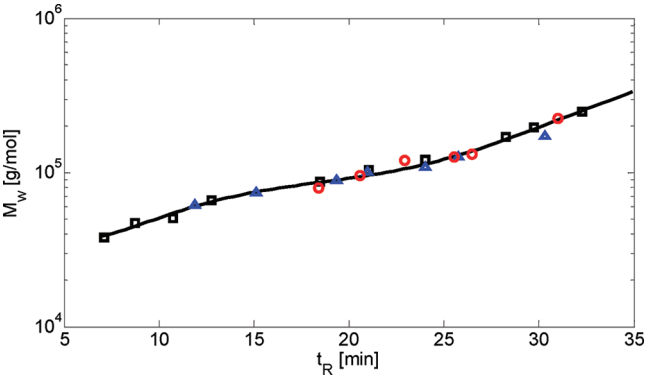

Figure 5. Calibration curve. The data have been determined on sample α (Δ) and β (o) and on one additional sample ($\square$). The latter sample is another exact comb structure with a branch grafted not in the middle of the backbone as in sample-β, but in the $^1/_3$-position from one end.[28] This sample is not discussed further in this work.

On the basis of the above calibration curves, the molecular weight distributions of the exact combs α and β were obtained consistently, as shown in Figure 6. Indeed, since samples α and β were obtained from exactly the same three-arm star molecules (see parts 3a and 3b in Figure 2), we expect that some of the distribution peaks are localized at the same molecular weight.

As shown in Figure 6, the distribution peaks are very narrow when expressed as a function of the molecular weight, and their optimum fitting results in the tiny polydispersity of about 1.004.

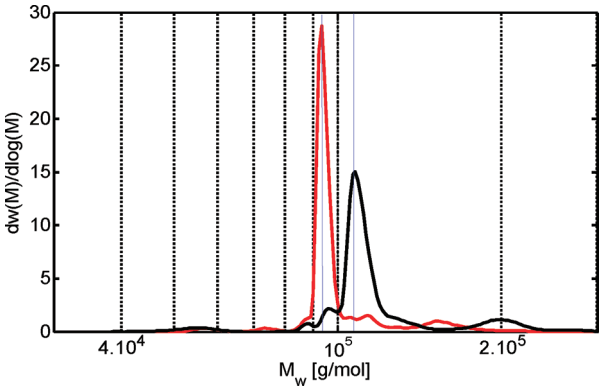

Figure 6. Normalized MWD of the exact combs α and β, based on the TGIC data and the calibration curves shown in Figure 5.

At a glance, this value may appear to be extraordinarily low but it is larger than the polydispersity value of Poisson distribution, which well represents the molecular weight distribution of anionic-polymerized samples without side reactions.[22,32] This value of H is below the resolution of SEC, which yielded a polydispersity of the linear parents around 1.02.[28] This again shows the sensitivity and capabilities of the TGIC technique, and of course the high purity in the synthesis procedure for linear precursor chains. From the TGIC curves, one can also observe that only a few structures with molar masses below 80 kg/mol are detected, which correspond to the tailing in the SEC chromatogram (see Figure 4). From the peak values of the main distributions, molar masses of 95 kg/mol and 106 kg/mol were determined for samples α and β, respectively. These values are very close to those reported from the synthesis, i.e., 94.4 kg/mol and 104.4 kg/mol, respectively (Table 1).[28]

IV.1.2. Experimental MWD of the Fractionated Samples. In Figure 7a, the MWD of the fractionated sample α is compared to the distribution of the unpurified sample. While the distribution of the mother sample is normalized following eq 4, the normalized MWD of the fractionated samples were multiplied by a constant 0.82 in order to match the main peaks of the mother samples (i.e., so that the area below the distribution curve equals 1, which means 100% of the polymer). Therefore, the fraction of target α-structure in the mother α-comb sample is 82%. By applying the same procedure for sample β, it is found that the fractionated β sample represents 70% of the mother sample. However, we suspect that this fractionated β-comb contains a few other structures in addition to the target one.

Indeed, from careful inspection of the curves of Figure 7b, the distribution of the fractionated sample β is clearly broader than the distribution of the fractionated comb α, which appears contradictory to the conclusion from section III.2, according to which the polydispersity of a specific species should decrease with the increase of its molecular weight. Therefore, we could suspect that the main peak of the MWD of the mother sample β corresponds to different architectures, and not only to the target exact β-comb polymer structure. Moreover, this distribution is extended toward longer times, i.e. larger masses, which means that the fraction β does not necessarily contain a large amount of target molecules, but rather larger molecules (different structures, see Figure 3). This conforms to the fact that, compared to α-comb, the β-comb sample was more difficult to fractionate cleanly due to the large amount of side products having similar MW to the main peak as can be seen in Figure 4d. Given the fact that the molar

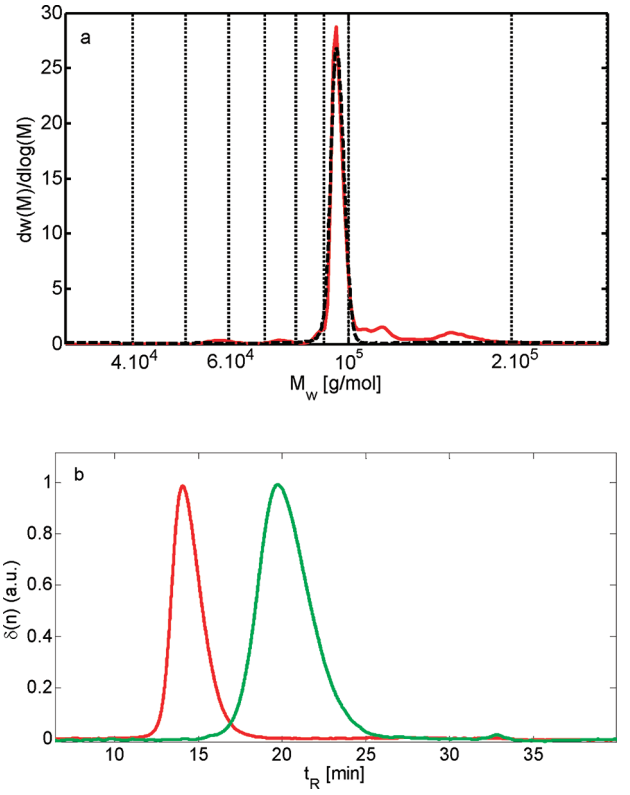

Figure 7. (a) Comparison between the MWD data of the unpurified and the IC-fractionated α-sample versus M_w (from the calibration as discussed in the text), obtained from TGIC measurements. (b) TGIC data for the two fractionated α- and β-samples versus elution times.

mass of a branch is 10.8 kg/mol, i.e. about 10% of the total molar mass of the exact β-comb (Table 1), and hence the different architectures have very similar molar masses, one can appreciate the difficulty of fractionating only the exact β-comb architecture.

IV.1.3. Decomposition of the MWD for the Exact α-Comb Polymer. On the basis of the statistical approach described in section III.1, we can now attempt to analyze the composition of the comb polymer α. To this end, we first had to determine the MWD of the parent polymers, i.e. the branches and the half-backbone, in order to correctly predict the localization and shape of the different peaks. Here, we approximate these distributions by considering log-normal distributions. As already mentioned above, their corresponding (weight-average) molar masses were fixed to 10.8 kg/mol and 25.6 kg/mol for the branches and the half-backbones (see section III.1), respectively, whereas their polydispersity was fixed to 1.004. These molar masses are very close to those reported in the synthesis paper, i.e., 11 kg/mol and 25 kg/mol, respectively.[28] Next, using these assumed MWDs, the MWD of all possible side-products (see for example Figure 3) of the exact α-comb sample are calculated (without any degree of freedom), and their respective fractions adjusted in order to fit the experimental TGIC data. Results obtained in such a way for the exact α-comb sample are shown in Figure, 8. To appreciate the complexity of the problem and sensitivity of the TGIC in detecting different structures, the distribution is also shown in a log−log plot. In such a representation, the presence (and exact position) of distribution peaks coming from side-products which are not listed in Figure 3b, are shown. It should be noted, however, that signals with strength below 10^{-3} are not taken into account as they are not properly resolved.

dx.doi.org/10.1021/ma2013805 |*Macromolecules* 2011, 44, 8631–8643

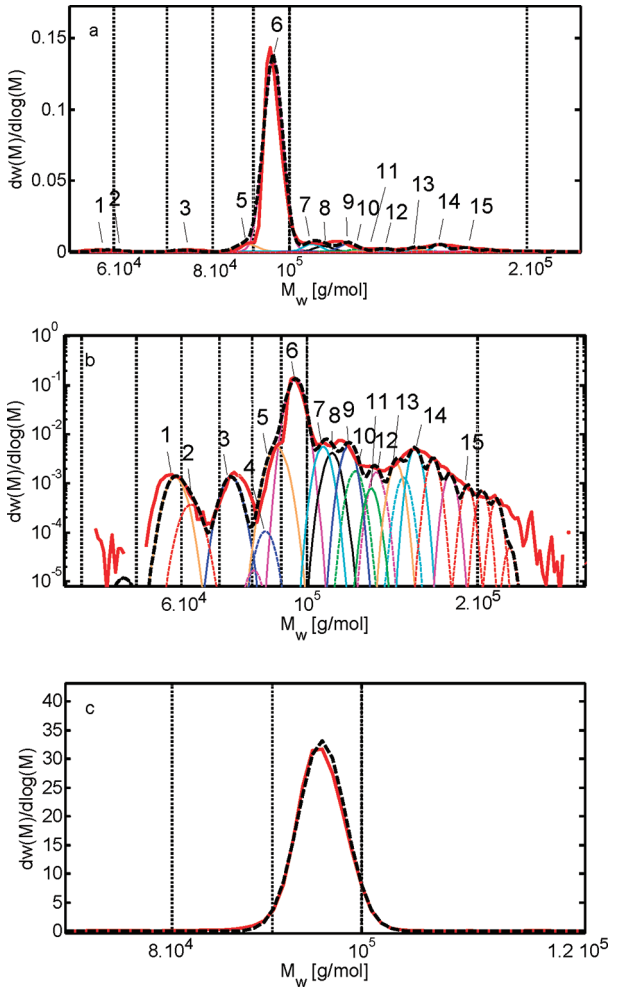

Figure 8. Comparison between the theoretical (thick --) and experimental (thick continuous) MWD of the mother α-sample, in a lin−log- (a) and log−log (b) presentation. Theoretical curves have been decomposed into different side-products, with their numbers corresponding to the architectures of Figure 3b. (c) Comparison between the theoretical (--) and experimental (continuous curve) MWD of the fractionated α-sample. For the theoretical curve, only the target fraction 6 of Figure 3 or Table 2 is accounted for.

From Figure 8a, one can remark that the first peak (1) of the MWD does not correspond to the half-molar mass (in reference to the target structure), in contrast to what could be concluded based on the SEC data (Figure 4a). Since this value of the molar mass corresponds to the limit of the calibration curve (Figure 5), it is difficult to judge whether this difference comes from the inaccuracy of the location of this peak. But since it only represents 1% of the sample (see Table 2), this should not strongly affect the conclusions. We also observe that only few large molecular structures with non-negligible fractions, based on four half-backbones are present in the mother sample, consistent with the original expectations (section III.1).

An important outcome from Figure 8c is the very favorable comparison of the experimental MWD of the fractionated α-comb sample to that predicted statistically from the theoretical MWD of the branches and the half-backbones, as described above (see also Figure 8b). This gives confidence about the theoretical predictions, which consistently indicate that the fractionated α-comb sample contains indeed only one kind of

Table 2. Determined Fractions (in %) of the Different Structures in the Original (Unfractionated) Exact Combs Based on Peak Analysis of the TGIC Signals[a]

	fraction														
sample	1	2	3	4	5	6	7	8	9	10	11	12	13	14	15
Comb α	1.0	0.3	1.0	-	3.8	82		3.2	2.4	2.8	0.4	0.01	0.6	1.3	2.3	0.45
Comb β	1.2	-	-	-	3.0	7.5	55	12	7.2	3.2	2.0	1.5	1.0	0.5	1.0	

[a] Fraction numbers refer to Figure 8b.

(target) architecture. This result can be quantified further. Indeed, the different components of the unfractionated mother sample and their fractions are listed in Table 1 (fraction numbers refer to Figure 8b). The target α-comb architecture represents 82% of the mother sample (i.e the purity of this sample is 82%). This confirms the state-of-the-art synthesis of these structures and marks a great improvement in the field. Recent work of similar analysis of H-type polymeric structures reported a purity of about 40%.[27] As already mentioned above, it must be emphasized that one cannot distinguish the difference between two molecules with the same number of branches and half-backbones, i.e. same total molar mass but different structure. Therefore, despite the fact that we may estimate how many branches they have, we cannot be sure about their correct localization. From the above analysis and the different possible architectures present in the sample (see also Figure 3), we infer that most of the molecules contain two half-backbones, as expected. The above analysis also suggests that a non-negligible number of molecular structures (about 5%) contain three branches fixed to a half-backbone instead of two (as, for example, architectures 9 in Figure 3). This could be explained from the synthesis procedure. There are also some incomplete or originally unforeseen architectures (for example, architectures 2, 3, and 5 in Figure 3). The possibility that some of these architectures are eluted very close to the target architecture 6 (Figure 3) cannot be excluded.

IV.1.4. Decomposition of the MWD for the Exact β-Comb. From the synthesis procedure (Scheme 1), we already know the theoretical MWD of the parent linear polymers, which should be identical to those determined for the α-comb sample. This strongly reduces the degrees of freedom in order to fit the experimental TGIC curve, since only the proportions of the exact β-comb and its side-products must be defined. The results obtained under these constraints are presented in Figure 9 and the different fractions listed in Table 2.

As with the exact α-comb sample, the agreement between theoretical and experimental MWD is satisfactory. From inspection of the distributions of Figure 9, the following observations can be made in reference to the architectures of Figure 3: First, the main peak mainly contains the target β-comb structure (architecture 7 in Figure 3), which represents 55% of the mother sample. In addition, it also contains 12% of architecture 8 and 7.2% of architecture 9. Second, the distribution peak corresponding to the α-comb sample (architecture 6) is also present and represents 7.5% of the mother sample. Third, as already observed in Figure 4, there is a large peak which corresponds to high-molecular-weight components and represents a fraction of about 5% of the mother sample. Such components represent architectures with three or four half-backbones. Moreover, since this peak is very large, several different architectures are needed in order to predict it accurately; clearly, one architecture alone is insufficient.

On the other hand, one should bear in mind that the real shape of this peak is questionable because it covers the high-molecular-weight region where the calibration curve is not very accurate (Figure 5) and, in addition, the predicted polydispersity of the corresponding molecules is very low (below the resolution limit of the experimental data, as already discussed).

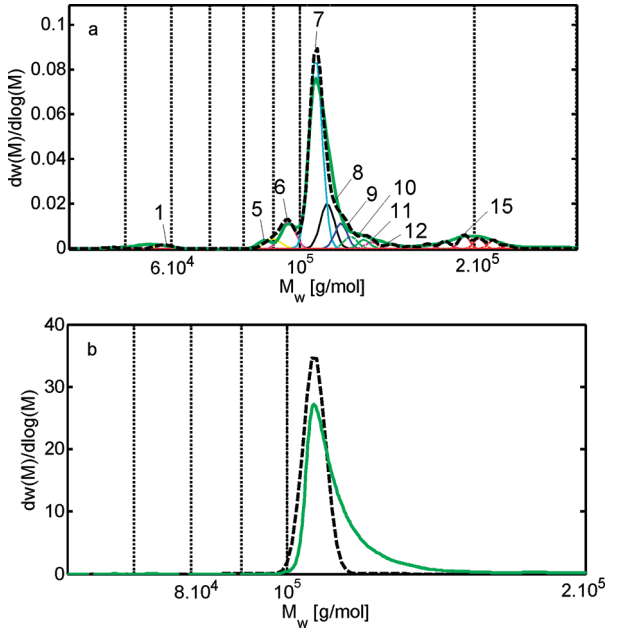

Figure 9. (a) Comparison between the theoretical (thick --) and experimental (thick continuous) MWD of the mother β-sample, in a lin−log presentation. Theoretical curves have been decomposed into different side-products, with their numbers corresponding to the architectures of Figure 3b. (b) Comparison between the theoretical (--) and experimental (continuous curve) MWD of the fractionated β-sample. For the theoretical curve, only the target fraction 7 of Figure 3 or Table 2 is accounted for.

From the above we conclude that, contrary to the fractionated α-comb sample, and in agreement with the discussion based of Figure 7b, the fractionated β-comb sample cannot be described by only one architecture, i.e., the target architecture 7 of Figure 3, and seems to include larger molecular structures. The latter appear responsible for the disagreement between theory and experiment.

IV.2. Rheology: Experiments and Modeling. In the previous section, the real composition of the exact combs α and β was extracted from the analysis of their MWD. Here, we attempt at extracting this information from the analysis of their linear viscoelastic response. To do so, we first compare the experimental data obtained with the unfractionated mother and fractionated target samples. Then, with the help of a tube-model theory, we analyze the results quantitatively.

IV.2.1. Experimental Linear Rheology. Master curves of the frequency-dependent storage (G') and loss (G'') moduli of the exact combs α and β and of the corresponding fractionated samples, along with the more sensitive loss angle ($\tan\delta = G''/G'$), are presented in Figure 10, parts a and b, respectively. First, a few remarks concerning the data are in order: The master curves were obtained with shift factors that matched those used with other 1,4-polybutadiene architectures, as shown in Figure 11. This confirms the quality of the data. On the other hand, it can be noted that the data in the region around the low-frequency minimum of $\tan\delta$, on approaching the terminal regime, do not superimpose perfectly. Despite our efforts with repeated measurements and annealing of the samples, we did not manage to improve this discrepancy. Hence, even if we wish to attribute this problem to the samples, its origin remains elusive. This discrepancy seems more pronounced in the α-comb sample, and in both cases it

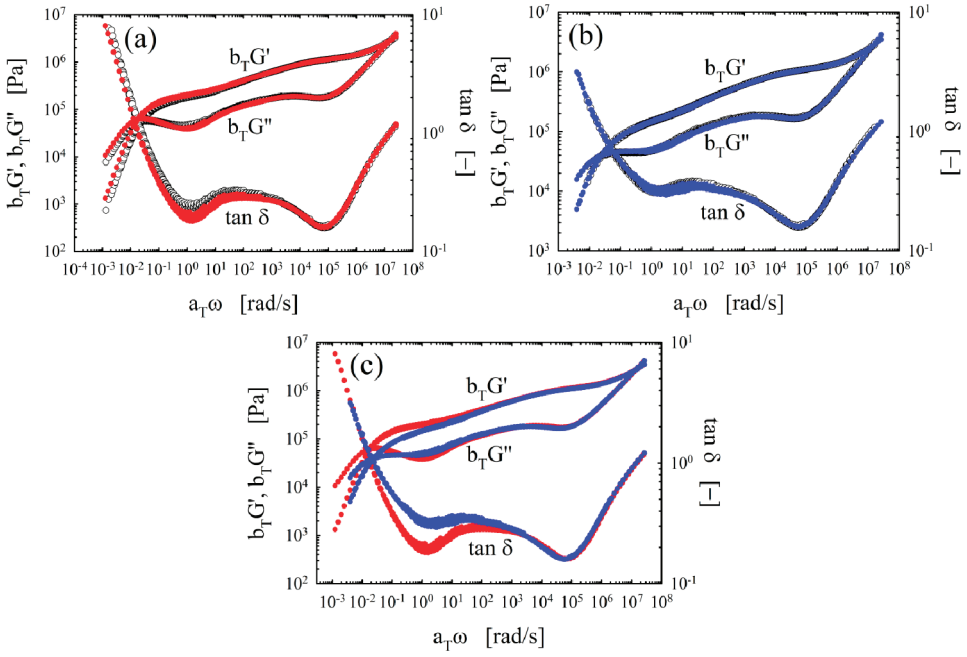

Figure 10. Master curves for the storage (b_TG') and loss (b_TG'') moduli and loss angle ($\tan\delta$) as a function of angular frequency ($a_T\omega$) for the mother samples and the fractionated samples ($T_{REF} = 20\ ^\circ C$). In part a, the results for the α-comb are shown: (○) unfractionated α-comb; (red ●) fractionated α-comb. In part b, the analogue is shown for the β-comb: (○) unfractionated β-comb (blue ●); fractionated β-comb. In part c, the fractionated α-comb and β-combs are directly compared to each other: (red ●) fractionated α-comb; (blue ●) fractionated β-comb.

dx.doi.org/10.1021/ma2013805 |*Macromolecules* 2011, 44, 8631–8643

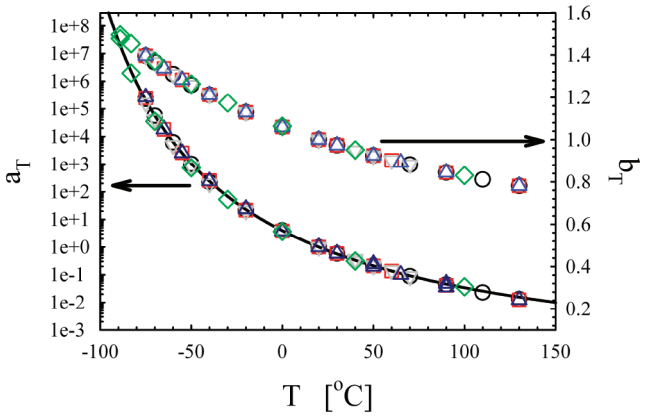

Figure 11. Vertical (b_T) and horizontal (a_T) shift factors and corresponding fit with the WLF equation as a function of temperature (T). Legend: (○) unfractionated α-comb; (red □) fractionated α-comb; (▽) unfractionated β-comb; (blue △) fractionated β-comb; (—) WLF-fit; (green ◇) PBD-LC1 (comb) from Kapnistos et al.[13]

appears in both unfractionated and fractionated samples. We note however that, to our experience and despite the difficulty in obtaining good data in that regime, such an effect is encountered reasonably frequently in (raw, unsmoothed) linear viscoelastic data of model macromolecular architectures.[5,13,17,33,34] On the other hand, the perfect superposition of the high-frequency data (reflecting local modes) as well the high-frequency plateau region for different samples, testifies the good quality of the data and confirms the very similar content of 1,4-microstructure. As already mentioned, and established in literature,[5,7,13,33] the data are characterized by two broad relaxations (minima in G'' or tan δ), which correspond to the hierarchical relaxation of the faster branches (around $a_T\omega = 6 \times 10^4$ rad/s) and the backbones which follow-up, at lower frequencies. Moreover, the G' value corresponding to the slow backbone relaxation is much smaller compared to that of the faster branch relaxation (effective plateau values), confirming the action of the tube dilation mechanism.[17] For all samples measured, the terminal regime has been reached. Remarkably, from Figure 10 very little difference is observed between the moduli of the mother and the purified (fractionated) $\alpha-$comb samples, and nearly none for the β-comb samples. Note that a representation of the data in the form of the so-called van Gurp-Palmen plot (of loss angle vs complex modulus), which is often considered more sensitive,[35,36] does not reveal a clearer picture (plots not shown). This is particularly surprising for the latter exact comb, which contains a larger amount of side-products, as discussed above. Hence, based on these experimental data only, one may be tempted to conclude either of t he three possibilities: (i) the samples tested are entirely pure, (ii) the presence of the particular side-products does not influence the rheology appreciably, (iii) rheology is not sensitive enough. The latter is clearly not true.[26] It turns out that, simply put on a qualitative basis, the presence of different structures as discussed in section IV.1.4 may result in a cancellation of contributions in the sense that structures with more branches may relax faster due to dilution, whereas structures with longer backbones relax slower, and the next effect may be negligible. This general idea, i.e. the combination of different relaxation mechanisms of the side products with different strengths will be further elucidated below.

In Figure 10c, the relaxation moduli of the fractionated comb samples α and β are compared. This comparison is rather interesting. Following the dilution idea, and assuming a single target structure, one can obtain estimates for the volume fraction of the backbone, $\varphi_{backbone}$ from the moduli data following $G_{low\ frequency\ plateau} = G_N^0 \varphi_{backbone}^{\alpha+1}$, with G_N^0 being the high-frequency plateau corresponding to the branch relaxation, as discussed above. Taking the plateau moduli as the values of the elastic modulus G' at the minima of tan δ and assuming a value of 1 for the dilution exponent α,[33,37] we obtain values for the backbone volume fraction $\varphi_{backbone}$ of 0.44 for the fractionated α-comb and 0.42 for the fractionated β-comb. However, if we now consider the values of the molar masses of the branches and half-backbones as discussed in section IV.1.3 (10.8 kg/mol and 25.6 kg/mol, respectively) in order to describe the structures of the target molecules, we obtain volume fractions of the inner part of the backbone, $\varphi_{backbone}$, equal to 0.55 for the α-comb and 0.49 for the β-comb. Whereas the experimental determination of the plateau moduli may slightly influence this comparison, the difference is undisputable, leading to larger estimated value in comparison to the experimental one obtained from rheology. In particular, a relative comparison of the two target structures suggests that, since the β-comb is essentially the α-comb with one extra branch in the middle, the dilution effect should be 6% higher for the β-comb, which is not observed from the experimental data where a difference of only 2% in the dilution effect is observed. This conforms to the suggestion that one of the two fractionated combs is not pure. Note that the same conclusion is drawn if a value of $^4/_3$ is used for the dilution exponent α.[33,38] On the other hand, looking now at the mother samples, the respective fractions for the unfractionated samples are 0.42 and 0.39, respectively. Hence, fractionation slightly shifts these values up, as can be also observed from Figure 10c. This result appears consistent with the modeling analysis to be presented below, suggesting that fractionation effectively weakens the dilution. Despite the sensitivity of rheology to the presence of side-products,[26] we note however that the present results do not show a strong sensitivity of the second plateau to fractionation, pointing to possible mutual cancellation of contributions of different side-products to the rheological signal. This will be further discussed below in conjunction to modeling. These results also show the different sensitivity of the rheological results and those from the TGIC analysis, especially for the β-sample (section IV.1.4).

IV.2.2. Comparison of Predicted and Experimental Viscoelastic Data. ***IV.2.2.1. Analysis of the Fractions.*** Assuming that the different fractions are entirely pure, and given the model's ability to provide quantitative predictions of the rheology of these exact comb polymers, a very satisfactory agreement is found between predicted and measured viscoelastic spectra, as can be seen in Figure 12. Nevertheless, one can observe discrepancies with both samples, and in particular with the β-comb sample.

The model predictions were obtained using the material parameters M_e = 1520 g/mol, G_N^0 = 1.2 MPa (obtained from the experimental data as the G' value corresponding to the high-frequency minimum of G'' or tan(G''/G')), and $\tau_e = 2 \times 10^{-7}$ s, and a dilution exponent $\alpha = 1$. These values are consistent with those used in the literature[17] and with the definition $G_N^0 = (4/5)\rho RT/M_e$, with ρ the density. We can see that, whereas the relaxation times corresponding to the branch and backbone relaxation are correctly predicted, the diluted backbone plateau of the α-comb sample is clearly above the experimental data (Figure 12a). From this observation alone, it is difficult to conclude about the origin of this discrepancy. Since the target fraction of the α-comb

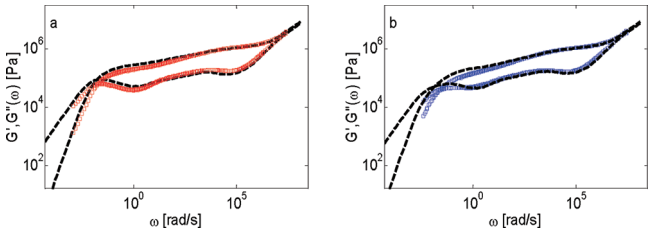

Figure 12. Experimental (purified samples) and predicted storage and loss moduli of the exact combs α (a) and β (b).

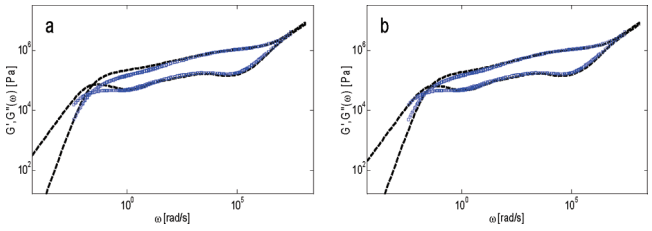

Figure 13. Comparison between theoretical and experimental data (on purified samples). Predictions are obtained by (a) considering 90% of target β-combs and 10% of half-molecules (b) the composition determined from the analysis of the MWD curve, with 65% of molecule 7, 20% of molecule 8, 9% of molecule 9, 4% of molecule 10, and 2% of molecule 11 (Figure 3b).

appears pure (see Figure 8c), it is tempting to attribute the discrepancy to the model and in particular to the chosen value of the dilution exponent α. However, we do not change this value here as we wish to keep the same one for both samples for consistency and for consistency with earlier works where a dilution exponent of 1 was found to yield excellent agreement between model and experiment.[5,6,13,33] On the other hand, as shown in Figure 12b, the difference between predicted and measured relaxation moduli is much larger for the exact β-comb sample, and cannot be corrected by slightly varying the model parameters. On the basis of only the rheological data, we can attribute the difference to the presence of half-molecules which speed-up the relaxation of the target structures. This in fact can be tested with the model. Indeed, as shown in Figure 13a, accounting for 10% of half- molecules (star-like as in Figure 2) is enough to obtain a much better agreement between predicted and experimental data (Figure 9a).

From the above, it becomes clear that, the sample contains a larger proportion of branches, which will enhance the level of the fast relaxation peak and thus, decrease the level of the slow relaxation peak corresponding to the relaxation of the backbone. This is illustrated in Figure 13b, where the composition of the fractionated sample is chosen as to be similar to that obtained from the fit of the TGIC MWD of the fractionated β-comb (Figure 9b). The comparison of experiments and predictions is again very satisfactory. Hence, a more detailed analysis of the MWD is in general needed in order to identify all different structures and analyze the rheological data accordingly. We also note that in the present modeling analysis we chose to simply add-up the contributions of different structures to the total viscoelastic sprectrum. We believe that this is a reasonable approximation as long as the main structure is the dominant fraction of the investigated sample and all other fractions are truly small.

IV.2.2.2. Influence of Side Products. As already mentioned in reference to Figure 10, the presence of different side products does not necessarily affect the rheological behavior of these model branched polymers. In the present case of exact combs α and β, there is barely any effect observed. In order to validate this result quantitatively, the different relaxation behaviors of specific architectures are studied and compared here, based on the model predictions.

First, the importance of reptation contribution to the overall relaxation of the samples is investigated. To this end, the predicted rheology of architectures based on two or on three half-backbones (archtectures 6 and 11, respectively, in Figure 3) are compared in Figure 14. While the fluctuation times of these molecules are identical (branch relaxation), only the molecules based on two half-backbones can relax by reptation. Therefore, the difference between the predicted viscoelastic curves provides an indication about the importance of the reptation process. As shown in Figure 14, the influence of reptation is rather small: the larger structures based on three half-backbones, which have been detected in the MWD of the mother samples (see Figure 9 and discussion) relax very similarly to the target exact β-comb architecture.

Furthermore, in order to investigate the role played by possible extra branches, the rheological data predicted for the monodisperse exact α-comb and for the same architecture with three additional branches in the middle and at the extremities of the backbone (the two architectures 9 of Figure 3) are compared in Figure 15.

We first observe that the main effect of the additional branches is the decrease of the level of the second, slow backbone plateau of the storage modulus, as expected because of the action of the dilution mechanism. We can also observe that the additional branches slightly hasten the relaxation of the backbone. This suggests that the extra solvent effect due to these branches is more important that the extra friction they bring along, which is responsible for slowing-down the reptation process. This result should not come as a surprise if one considers the outcome of Figure 14, i.e., that reptation does not play an important role for these exact comb architectures, and the fact that contour length fluctuations of the inner part of the backbone do not require the motions of this middle branch. Note further that, since the fluctuation times of the α-comb sample, with or without extra branches in the middle, are similar, in this case constraint release is found to be the dominant relaxation mechanism.

IV.2.2.3. Influence of the Star Architectures. As a last test, it is interesting to compare the relaxation times of a simple branch to the relaxation times of the exact comb molecules. Indeed, as shown in Figure 3, branches of several length can be found among the possible architectures, often due to incomplete synthesis of some molecules. Their molar mass varies between 10.8 kg/mol (i.e., the expected molar mass for a branch) to 36.4 kg/mol (i.e., the molar mass of a long branch composed of an half-backbone of 25.6 kg/mol plus a normal branch of 10.8 kg/mol). As shown in Figure 16, while the relaxation times of the expected branches (of M_w = 10.8 kg/mol) are relatively short, the terminal relaxation time of the long branches (of M_w = 36.4 kg/mol) are similar to the terminal relaxation time of the exact α-comb molecules. This is not surprising since as explained above, the extra-friction brought by an extra branch is compensated by a larger dilution effect. However, the shape of the storage modulus predicted by considering only one generation of branches, which shows a one-step relaxation process, is very different from the storage modulus of the α-comb sample, which shows a two-step, hierarchical, relaxation.

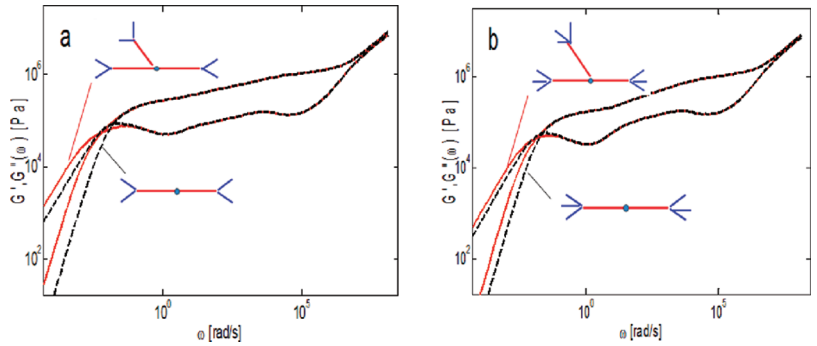

Figure 14. Comparison between predicted moduli, by considering: (a) architectures composed of two (--) or three (continuous lines) half-backbones, each one having two branches end-grafted (i.e., architectures 6 or 11 of Figure 3b) and (b) architectures composed of two (--; structure 8b of Figure 3b) or three (continuous lines) half-backbones, each one having three branches end-grafted.

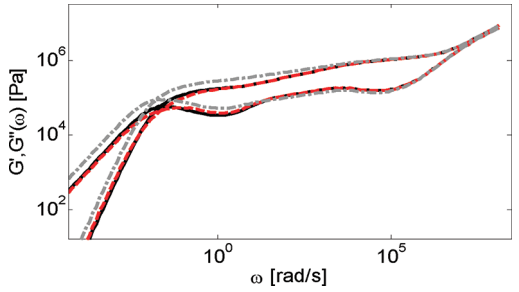

Figure 15. Predicted storage and loss moduli of monodisperse architectures 6 (-·--·), 9a (--), and 9b (continuous) from Figure 3.

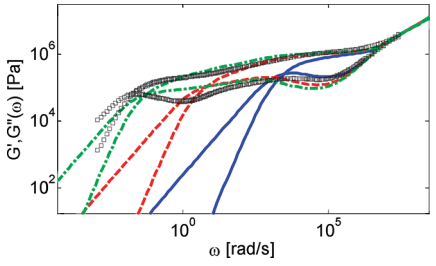

Figure 16. Comparison between experimental storage and loss moduli of the fractionated α-comb (□) and the predicted moduli of star-like molecules with arm molar mass of 10.8 kg/mol (—), 25.6 kg/mol (--) and 36.4 kg/mol (-·-).

IV. 2.2.4. Comparing Fractionated and Unfractionated (Mother) Samples. From the above modeling analysis it becomes evident that the presence of different structures in the exact comb samples (side products) can contribute either to faster relaxation (as in Figure 15), or to slower relaxation (as in Figure 14), depending on their architecture and fraction. Therefore, by properly combining such "slower" and "faster" molecules, their overall influence can be mutually compensated. This can explain why the viscoelastic spectra of the unfractionated mother samples are so similar to the fractionated target exact combs. For the particular case examined here, this is rather a coincidence and does not diminish the sensitivity of rheology. On the contrary, it underlines the need to combine different techniques of different sensitivities in order to explore the detailed response of such complex macromolecules. Note further that, for the α-comb, the comparison between the model predictions with a single target structure and the experimental rheology data are improved upon fractionation. This also holds for the β-comb, although in the latter case the improvement is negligible, even not visible for the large scales on which the data are plotted here. A careful examination of the values shows nevertheless a clear improvement for both combs.

V. CONCLUDING REMARKS

The significant advances of the last 2 decades in the field of entangled branched polymers render the synergy of synthesis, physical experiment and modeling a mandatory task for any further development. Moreover, the tremendous progress in chemistry has allowed exploring fine details of polymeric response, which prompted further progress. Currently, a grand challenge is to better understand the role of polydispersity and in particular structural polydispersity. Even the state-of-the-art synthesis cannot escape the unwanted presence of small amounts of side products. To this end, advanced characterization techniques come to the rescue. In particular, interaction chromatography is now established as an indispensable tool for addressing the detailed response of architecturally complex polymers.

In this work we have investigated the role of architectural dispersity on the rheology of model exact comb polymers, i.e., well-defined polymers with a priori known position of a single branch. We have shown that, to understand the relationship of polymer structure and macroscopic response it is imperative to uniquely combine 4 major expertises: synthesis, characterization, rheology, and modeling. We note that characterization needs both SEC and TGIC, whereas modeling needs both a statistical approach for predicting the distribution of molar mass and a predictive tool for the rheology. A tedious, elaborate coupling of these techniques leads to the following results:

High-vacuun anionic synthesis remains the state-of-the-art technique for well-defined macromolecular architectures. Even so, side-products cannot be avoided, but we note significant progress over earlier attempts. One may then ask the philosophical question "how model are model polymers"? With the present technique, the answer is "as model as you can get". The present work has also reported remarkable advance in terms of product purity over recent similar efforts.[27]

TGIC makes the difference in the analysis of the structures, but the calibration of elution times with molar mass is very delicate and can be a source of errors. SEC is a necessary complementary analytical tool, although it cannot correctly measure samples with very small polydipsersity, and the peaks of the MWD cannot be clearly distinguished.

Whereas rheology is the main tool for characterizing entangled branched polymers, for complete understanding it must be complemented by other techiniques and, by the same token it nicely complements chromatographic techniques. The particular example of this work, i.e., the analytic comparison of the two structures of H-polymer and H-polymer with 1 additional branch in the middle demonstrates the fine differences in sensitivity of the different techniques and the power of combining all in order to resolve the problem quantitatively and self-consistently. It is essential to recall that the big picture in this field is to design strcutures for desired rheology. Hence, we believe that an important, albeit alarming conclusion is the nearly identical viscoelastic response of unfractionated and fractionated samples with different structures but mutual cancellation of effects. This also proves the significance of tube modeling for obtaining deeper understanding, as well as of the fractionation for testing or confirming predictions.

AUTHOR INFORMATION

Present Addresses

○ MedImmune LLC, Gaithersburg, MD.

ACKNOWLEDGMENT

We acknowledge support by the EU through the ITN DYNACOP (grant 214627). E.v.R. thanks Fonds National de la Recherche Scientifique (chargé de recherche) for partial support. T.C. acknowledges support from NRF via NRL (R0A-2007-000-20125-0), SRC (R11-2008-052-03002), and WCU (R31-2008-000-10059-0) programs. J.P. acknowledges the hospitality and support of FORTH.

REFERENCES

(1) McLeish, T. C. B. *Adv. Phys.* **2002**, *51*, 1379–1527.
(2) McLeish, T. C. B. *Europhys. Lett.* **1988**, *6*, 511–516.
(3) Das, C.; Inkson, N. J.; Read, D. J.; Kelmanson, M. A.; McLeish, T. C. B. *J. Rheol.* **2006**, *50*, 207–235.
(4) Larson, R. G. *Macromolecules* **2001**, *34*, 4556–4571.
(5) McLeish, T. C. B.; Allgaier, J.; Bick, D. K.; Bishko, G.; Biswas, P.; Blackwell, R.; Blottiere, B.; Clarke, N.; Gibbs, B.; Groves, D. J.; Hakiki, A.; Heenan, R. K.; Johnson, J. M.; Kant, R.; Read, D. J.; Young, R. N. *Macromolecules* **1999**, *32*, 6734–6758.
(6) van Ruymbeke, E.; Orfanou, K.; Kapnistos, M.; Iatrou, H.; Pitsikalis, M.; Hadjichristidis, N.; Lohse, D. J.; Vlassopoulos, D. *Macromolecules* **2007**, *40*, 5941–5952.
(7) Ahmadi, M.; Bailly, C.; Keunings, R.; Nekoomanesh, M.; Arabi, H.; van Ruymbeke, E. *Macromolecules* **2011**, *44*, 647–659.
(8) Watanabe, H.; Matsumiya, Y.; van Ruymbeke, E.; Vlassopoulos, D.; Hadjichristidis, N. *Macromolecules* **2008**, *41*, 6110.
(9) Nielsen, J. K.; Rasmussen, H. K.; Denberg, M.; Almdal, K.; Hassager, O. *Macromolecules* **2006**, *39*, 8844–8853.
(10) Zhou, Q.; Larson, R. G. *Macromolecules* **2007**, *40*, 3443–3449.
(11) McLeish, T. C. B.; Larson, R. G. *J. Rheol.* **1998**, *42*, 81.
(12) Inkson, N. J.; Graham, R. S.; McLeish, T. C. B.; Groves, D. J.; Fernyhough, C. M. *Macromolecules* **2006**, *39*, 4217.
(13) Kapnistos, M.; Vlassopoulos, D.; Roovers, J.; Leal, L. G. *Macromolecules* **2005**, *38*, 7852–7862.
(14) Larson, R. G.; Zhou, Q.; Shanbhag, S.; Park, S. J. *AIChE J.* **2007**, *53*, 542.
(15) Hassell, D. G.; Hoyle, D.; Auhl, D.; Harlen, O.; Mackley, M. R.; McLeish, T. C. B. *Rheol. Acta* **2009**, *48*, 551.
(16) Lee, K.; Mackley, M. R.; McLeish, T. C. B.; Nicholson, T. M.; Harlen, O. G. *J. Rheol.* **2001**, *45*, 1261.
(17) Kapnistos, M.; Koutalas, G.; Hadjichristidis, N.; Roovers, J.; Lohse, D.; Vlassopoulos, D. *Rheol. Acta* **2006**, *46*, 273.
(18) Crosby, B. J.; Daniels, R.; McLeish, T. C. B.; Mangnus, M.; de Groot, W. *J. Rheol.* **2002**, *46*, 401.
(19) Janzen, J.; Colby, R. H. *J. Mol. Struct.* **1999**, *485−486*, 569–584.
(20) van Ruymbeke, E.; Stéphenne, V.; Daoust, D.; Godard, P.; Keunings, R.; Bailly, C. *J. Rheol.* **2005**, *49*, 1503–1520.
(21) van Ruymbeke, E.; Coppola, S.; Balacca, L.; Righi, S.; Vlassopoulos, D. *J. Rheol.* **2010**, *54*, 507.
(22) Lee, W.; Lee, H.; Cha, J.; Chang, T.; Hanley, K. J.; Lodge, T. P. *Macromolecules* **2000**, *33*, 5111.
(23) Chang, T. *J. Polym. Sci., Part B: Polym. Phys.* **2005**, *43*, 1591.
(24) Ryu, J.; Chang, T. *Anal. Chem.* **2005**, *77*, 6347.
(25) Chambon, P.; Fernyhough, C. M.; Im, K.; Chang, T.; Das, C.; Embery, J.; McLeish, T. C. B.; Read, D. J. *Macromolecules* **2008**, *41*, 5869.
(26) Kapnistos, M.; Lang, M.; Vlassopoulos, D.; Pyckhout-Hintzen, W.; Richter, D.; Cho, D.; Chang, T.; Rubinstein, M. *Nat. Mat.* **2008**, *7*, 997.
(27) Li, S. W.; Park, H. E.; Dealy, J. M.; Maric, M.; Lee, H.; Im, K.; Choi, H.; Chang, T.; Rahman, M. S.; Mays, J. *Macromolecules* **2011**, *44*, 208.
(28) Nikopoulou, A.; Iatrou, H.; Lohse, D. J.; Hadjichristidis, N. *J. Polym. Sci., Part A: Polym. Chem.* **2009**, *47*, 2597.
(29) Ferry, J. D. *Viscoelastic Properties of Polymers*, 3rd ed.; Wiley: New York, 1980.
(30) Zoller, P.; Walsh, D.; *Standard Pressure-Vol.-Temperature Data for Polymers*: Technomic Publishing Co.: New York, 1995.
(31) van Ruymbeke, E.; Keunings, R.; Stephenne, V.; Hagenaars, A.; Bailly, C. *Macromolecules* **2002**, *35*, 2689.
(32) Ryu, J.; Im, K.; Yu, W.; Park, J.; Chang, T.; Lee, K.; Choi, N. *Macromolecules* **2004**, *37*, 8805.
(33) Kirkwood, K.; Leal, L. G.; Vlassopoulos, D.; Driva, P.; Hadjichristidis, N. *Macromolecules* **2009**, *42*, 9592–9608.
(34) Graessley, W. W. *Macromolecules* **1982**, *15*, 1164.
(35) Dealy, J. M.; Larson, R. G. *Structure and rheology of molten polymers*: Hanser Publishers: Munich, Germany, 2006.
(36) Trinkle, S.; Friedrich, C. *Rheol. Acta* **2001**, *40*, 22.
(37) Graessley, W. W. *Polymeric Liquids & Networks: Structure & Rheology*: Garland Science: New York, 2008.
(38) van Ruymbeke, E.; Watanabe, H. *Macromolecules* **2011** submitted.